

Predictive modeling and experimental implementation of organic acids in stream recovery by reactive extraction in membrane contactors

F. Chemarin, V. Athès, W. Buquet, M. Bedu, F. Allais, A.F. Teixeira, Marwen Moussa, Ioan-Cristian Trelea

▶ **To cite this version:**

F. Chemarin, V. Athès, W. Buquet, M. Bedu, F. Allais, et al.. Predictive modeling and experimental implementation of organic acids in stream recovery by reactive extraction in membrane contactors. Chemical Engineering Journal, 2022, 431 (part 2), pp.134067. 10.1016/j.cej.2021.134067 . hal-03516921

HAL Id: hal-03516921

https://agroparistech.hal.science/hal-03516921

Submitted on 1 Feb 2022

HAL is a multi-disciplinary open access archive for the deposit and dissemination of scientific research documents, whether they are published or not. The documents may come from teaching and research institutions in France or abroad, or from public or private research centers.

L'archive ouverte pluridisciplinaire **HAL**, est destinée au dépôt et à la diffusion de documents scientifiques de niveau recherche, publiés ou non, émanant des établissements d'enseignement et de recherche français ou étrangers, des laboratoires publics ou privés.

Predictive modeling and experimental implementation of organic acids *in stream* recovery by reactive extraction in membrane contactors

F. Chemarin[a,b], V. Athès[b], W. Buquet[a], M. Bedu[b], F. Allais[a], A. F.Teixeira[a], M. Moussa[b*], I.C. Trelea[b]

[a] URD Agro-Biotechnologies Industrielles (ABI), CEBB, AgroParisTech, F-51110 Pomacle, France

[b] Université Paris-Saclay, INRAE, AgroParisTech, UMR SayFood, F-78850, Thiverval-Grignon, France

* Corresponding author: marwen.moussa@agroparistech.fr

Abstract

Membrane-based reactive extraction as an *in situ* product recovery technique is a promising strategy for process intensification, in particular in the case of the bioproduction of organic acids. Reactive extraction allows a high selectivity for the extraction of the targeted acid and the microporous membrane keeps biocatalysts in the aqueous broth while implementing a large liquid-liquid surface area and ensuring a dispersion-free contact, without problems of emulsion formation. This paper deals specifically with the extraction of biobased 3-hydroxypropionic acid using tri-*n*-octylamine in *n*-decanol. In order to maintain an effective driving force for 3-HP transfer into the organic phase, this latter was continuously regenerated by recovering the acid in a back-extraction aqueous phase, giving a complete pertraction process. A mass transfer model for this process was developed. It is based on the boundary layer theory and takes into account chemical and physical equilibria of complexation/dissociation and partitioning, species diffusion in the membrane pores and viscosity variations in the organic phase. Viscosity highly depends on acid concentration, increasing up to 50% when 3-HP concentration reaches 28 $g.L^{-1}$. Thus, it was possible to predict different experimental results with $R^2 \geq 0.99$, totally neglecting chemical kinetics and interfacial resistance for both extraction and back-extraction steps. The model allows the prediction of extraction kinetics with (1) fixed initial concentrations and (2) with gradual 3-HP feed (mimicking a bioconversion) in transient and steady

states coupled with back-extraction (globally also called pertraction). Model based analysis of mass transfer mechanisms led to the construction of a nomogram giving 3-HP stationary concentration in the case of a typical production rate, enabling for example a rapid organic phase selection or membrane sizing.

Keywords : solvent extraction; membrane contactor; mass transfer modeling; extractive bioconversion; *in situ* product recovery; organic acids

Abbreviations:

3-HP: 3-hydroxypropionic acid

AH: non-dissociated acid

C_{org}: total concentration of 3-HP (CPX + AH_{org}) in the organic phase

CPX: acid-amine complex

d: diameter

D: diffusion coefficient

F: 3-HP feed rate in the extracted aqueous phase

J: molar flow ($mol.s^{-1}$)

k: mass transfer coefficient

K_{11}: complexation constant

K_A: dissociation constant of an organic acid

K_w: dissociation constant of water

L: length of the fiber

m: decanol/water partition coefficient

M: molecular weight

Q_{aq}: volumetric flowrate of the aqueous phase

Q_{org}: volumetric flowrate of the organic phase

r: reaction rate

R: rate constant

R_3N: tertiary amine

S: surface of transfer

T: temperature

TOA: tri-*n*-octylamine

v: molar volume

V: volume

x_{ROH}^{ini}: molar fraction of decanol in the *n*-decanol-tri-*n*-octylamine mixture

μ: dynamic viscosity

τ: residence time

φ: decanol volume fraction in the organic phase

Subscripts and superscripts:

aq: in reference to the aqueous phase

BE: in reference to the back-extraction side of the pilot

E: in reference to the extraction side of the pilot

fib: in reference to the global volume of the fibers

fibin: in reference to the internal volume of the fibers (lumen)

int: in reference to the liquid-liquid interface

lm: logarithmic mean

org: concerning the organic phase

shell: in reference to the shell side of the membrane module

1. Introduction

Reactive liquid-liquid extraction is an efficient way to recover acids from dilute aqueous phases [1]. In such a process, an extractant diluted in an organic phase is able to bind selectively to the acid in order to form a globally hydrophobic complex that is soluble in the organic phase. Most of the time, the extractant is a hydrophobic amine or a phosphorous-bonded oxygen donor. This process raised a lot of interest in the industrial sector for the purification of bio-based organic acids from fermentation broth, particularly for citric and lactic acids [2–4].

The use of reactive extraction as an *in situ* or *in stream* product recovery process has been widely studied to remove inhibition due to organic acids accumulation in fermentation broths. For example, in the case of lactic acid, higher yields, concentrations and productivities could be reached by continuously removing the acid from the broth during fermentation compared to a fermentation with acid accumulation [5–8]. The main issues in order to operate an extractive fermentation in the case of organic acids are the solvent toxicity and the compatibility between optimal fermentation conditions and pH for an efficient extraction. The direct contact between the microorganisms and the organic extraction phase can be noxious and even lead to the cell inactivation. To overcome solvent toxicity, the implementation of membrane-based reactive extraction for the continuous *in-stream* product recovery has been successfully performed using immobilized [9–11] or free cells [12–14]. In this kind of device, a phase (1) showing affinity for the membrane material can wet and fill the pores of the membrane. The other phase (2), showing less affinity towards the membrane material, is then maintained at the surface of the membrane without entering the pores due to a controlled overpressure ~~(P2>P1)~~. In practice, phase (2) first flows on one side and wets the membrane surface without entering the pores because of the lack of affinity with the membrane material, even with a reasonable overpressure applied. On the other side, phase (1) naturally fills the membrane pores because of the affinity with the membrane material. Accordingly, an overpressure applied on phase (2) blocks the outlet of the pores for phase (1) and prevents it from crossing the membrane. The contact between both phases is then made and the interface is stabilized at the mouth of the pores

where the complexation reaction between the acid and the extractant can take place. Accordingly, membranes with high porosities can lead to high specific surface area. It is a dispersion-free process that prevents emulsion formation. The small size of the pores limits the contact between microorganisms and the organic phase, potentially enhancing the biocompatibility of the process and maintaining suspended cells in the bioreactor [12].

Some historical organic acids like citric and itaconic acids are produced at low pH (~2-3) using fungi, but bacterial products like lactic acid need higher pH for cell maintenance. However, nowadays most large scale bio-based organic acids, like lactic acid [15], are industrially produced at low pH (~3) using modified yeasts. This makes fermentation and optimal pH for extraction compatible. Recently, industrial patents also reported the production of 3-hydroxypropionic acid (3-HP) at low pH using yeasts [16]. Nevertheless, despite the pH control around 4, 3-HP accumulation in the broth has been reported to inhibit cell growth and productivity [17]. In this context, the *in situ* or *in stream* reactive extraction of 3-HP using membrane contactors seems promising, particularly in hollow-fiber membrane contactors as they are known for their high porosity and high packing densities [18]. Deep understanding of dynamic behavior and accurate modeling are needed to predict process efficiency and acid accumulation during reactive extraction in membrane contactors, model that may further be used for scaling issues.

The most used models are based on the boundary layers theory. They usually rely on several local mass transfer coefficients to calculate the mass transfer from the aqueous to the organic bulk: on the aqueous side, in the membrane pores and on the organic side. Even if some authors have used distribution coefficients, in reactive extraction equilibrium is determined by complexation constants. Some authors [19,20] have reasonably modeled extractions without taking the interfacial reaction kinetics into account and some others found it necessary to predict results accurately. For example, Juang et Chen [21] modeled the membrane-based extraction of citric and lactic acids using tri-*n*-octylamine in xylene with two kinetic rate constants and concluded that chemical kinetic resistance could account up to 50 and 40% of the global extraction resistance for citric and lactic acids

respectively. Huang et al [22] needed to fit 3 kinetic rate constants to predict lactic acid concentration profiles in a pertraction system coupling extraction with Alamine 336 in 2-octanol and back-extraction with sodium hydroxide using two membrane contactors. They concluded that chemical kinetics could account for more than 71% and 94% of the global mass transfer resistance for extraction and back-extraction respectively. However, 94% of the resistance for a strong base neutralizing a weak acid seems quite high and reactions between acids and tertiary amines have often been found to be fast and occurring in thin diffusion films when no membrane contactors were used [23,24].

In this paper, we aim at developing a model for a hollow-fiber membrane-based reactive extraction of 3-hydroxypropionic acid by tri-*n*-octylamine in *n*-decanol with or without coupling a back-extraction step that simultaneously regenerates the extracting phase. We developed a model where interfacial reactions kinetics are neglected but where viscosity variations due to acid-amine complex accumulation in the organic phase are considered.

2. Material and methods

2.1 Modeling

2.1.1. Assumption of constant concentrations along the fibers

If the residence times of the phases in the fibers or in the shell side are much shorter than the characteristic times of extraction, the amount transferred in one pass is small compared to the initial amount and species concentrations can be considered homogeneous all along the fibers. This assumption will be checked in the results section. In cases when this assumption is not verified, concentrations variation along the module can be considered by discretizing the module length. Average residence times in the module for the aqueous (in the fibers) and the organic (shell side) phases were calculated as (with symbols detailed in Table 3):

$$\tau_{fib} = \frac{number\ of\ fibers\ \times internal\ fiber\ volume}{Q_{aq}} = \frac{9800 \times \pi \left(\frac{d_{fibin}}{2}\right)^2 L}{Q_{aq}} \sim 6\ s. \quad (1)$$

$$\tau_{shell} = \frac{Shell\ volume - number\ of\ fibers\ \times external\ fiber\ volume}{Q_{org}}$$

$$= \frac{\pi \left(\frac{d_{shell}}{2}\right)^2 L - 9800\pi \left(\frac{d_{fib}}{2}\right)^2 L}{Q_{org}} \sim 36\ s. \quad (2)$$

It appeared that average residence times were much lower than characteristic times of extraction which range between 2 000 and 7 000 seconds depending on extraction conditions (cf. section 3.2. Model calibration). The assumption of constant concentrations along the fibers thus appeared reasonable.

2.1.2. Chemical reactions considered in the model

The considered chemical reactions are the following (taken from [25]):

- Homogeneous reactions in the aqueous phase:

  $AH_{aq} + H_2O \leftrightarrow A^- + H_3O^+$ Acid dissociation (reaction 1)

  $2H_2O \leftrightarrow HO^- + H_3O^+$ Water autoprotolysis (reaction 2)

- Interfacial reactions at the liquid-liquid interface:

  $AH_{aq} \leftrightarrow AH_{org}$ Acid partitioning (reaction 3)

  $AH_{aq} + R_3N \leftrightarrow CPX$ Complex formation (reaction 4)

- Homogeneous reactions in the organic phase:

  $CPX \leftrightarrow AH_{org} + R_3N$ Complex dissociation (reaction 5)

The interface is supposed to be at chemical equilibrium, meaning that interfacial chemical reactions are much faster than species transfers. Equations related to chemical reactions are given in Table 1.

Table 1: Equations implemented in the model concerning chemical equilibria and kinetics

Equilibrium at the interface		
Reaction 1	$[A^-]_{int}[H_3O^+]_{int} - K_A[AH_{aq}]_{int} = 0$	(3)
Reaction 2	$[H_3O^+]_{int}[HO^-]_{int} - K_w = 0$	(4)
Reaction 3	$[AH_{org}]_{int} - m\varphi[AH_{aq}]_{int} = 0$	(5)
Reaction 4	$[CPX]_{int} - K_{11}[AH]_{int}[R_3N]_{int} = 0$	(6)
Reaction kinetics in the aqueous phase		
Rate of reaction 1	$r_1 = R_{-1}(K_A[AH_{aq}] - [A^-][H_3O^+])$	(7)
Rate of reaction 2	$r_2 = R_{-2}(K_w - [H_3O^+][HO^-])$	(8)
Reaction kinetics in the organic phase		
Rate of reaction 5	$r_5 = R_{-5}\left(\frac{m\varphi}{K_{11}}[CPX] - [AH_{org}][R_3N]\right)$	(9)

Here partial reaction orders are supposed to be 1, and R_{-1}, R_{-2} and R_{-5} are the backward rate constants of reactions 1, 2 and 5 respectively.

2.1.3. Mass fluxes

Most of the membrane extraction modeling relies on the boundary layer model. For extraction, the transport is separated into 5 zones: (i) the aqueous bulk phase, (ii) the aqueous boundary layer, (iii) the membrane pores, (iv) the organic boundary layer and (v) the organic bulk phase. A conceptual view of the boundary layer model is presented in Figure 1.

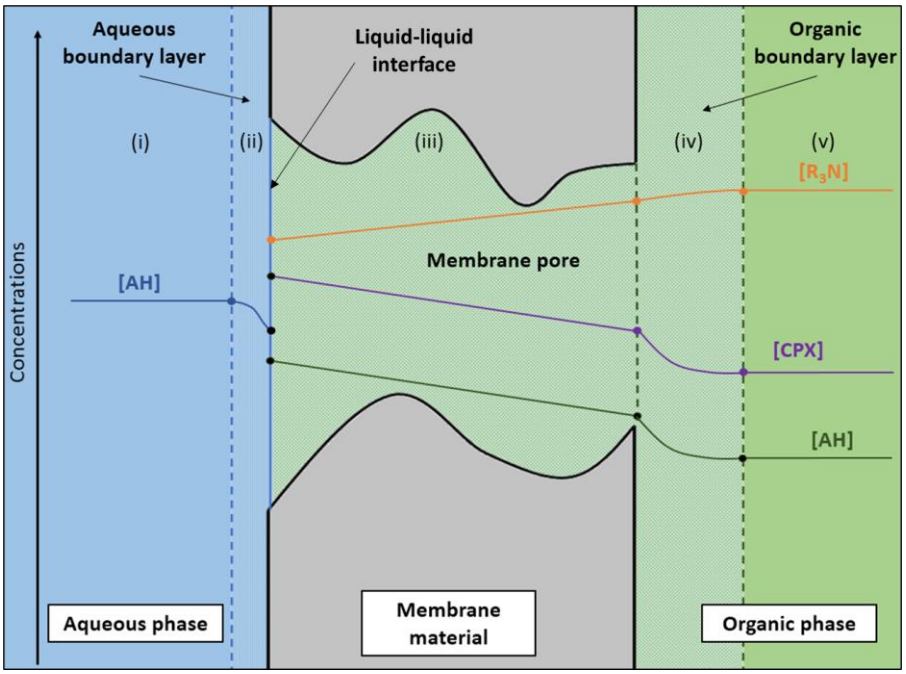


Figure 1: Conceptual view of the boundary layer model with concentration profiles

Membrane pores are filled with organic phase because of the hydrophobic membrane material. Concentrations are considered homogeneous in bulks and vary in thin films close to the membrane wall and inside the membrane pores. In boundary layers and in the membrane pores, the mass fluxes can be described by mass transfer coefficients and driving forces. In the present study, we merged zones (iii) and (iv) for the sake of simplification. Zone (iii), inside membrane pores, is supposed to have the major impact on the global transfer resistance. If no significant accumulation of species occurs in zones (ii) to (iv) due to their comparatively small volumes, then pseudo steady-state regime can be assumed, and the molar flow can be classically expressed as the product of the mass transfer coefficient, the surface open to the transfer and the driving force of the transfer :

$$J_X = \mathrm{k}_X S_X([X] - [X]_{int}) \quad (10)$$

Where:

- J_X is the flow of a given species X across the corresponding phase towards the interface
- k_X is the mass transfer coefficient of species X
- S_X is the surface open to the transfer of species X
- $[X]_{int}$ is the concentration of the species X at the interface

- [X] is the concentration of the species X in the corresponding bulk
- X is the transferred species, namely AH_{aq}, A^-, H_3O^+ and HO^- in the aqueous phase and AH_{org}, CPX and R_3N in the organic phase

Globally, the mass transfer path considered in the model is the following:

- Transfer of the aqueous reactants from the aqueous phase bulk (i) to the liquid-liquid interface through the aqueous boundary layer
- Transfer of the organic reactants from the organic phase bulk (v) to the liquid-liquid interface through the organic boundary layer and the membrane pores
- Instantaneous reactions 3 and 4 of the species at the interface (chemical equilibria as the interface continuity conditions)
- Transport of the reactions' products from the interface to the bulks
- Concentrations are assumed homogeneous in the bulks (fluids circulation) with homogeneous reactions 1 and 2 in the aqueous phase and reaction 5 in the organic phase

2.1.4. Mass balance equations

After chemical reactions and flux definitions, another condition is needed in order to solve the system: mass conservation. If we assume that the only accumulation of species in the system takes place in the bulk phases, mass conservation allows to relate interfacial molar flows between them on one hand, and bulk concentration variations with molar flows, chemical reactions and acid influx on the other hand. The mass balances used are given in Table 2.

Table 2: Equations implemented in the model concerning mass balance and molar flow conservation

Mass balance equations in the aqueous phase		
Protonated acid in the aqueous phase	$\frac{d[AH_{aq}]}{dt} = -\frac{J_{AH,aq}}{V_{aq}} - r_1 + F$	(11)
Dissociated acid	$\frac{d[A^-]}{dt} = -\frac{J_{A^-}}{V_{aq}} + r_1$	(12)
Hydronium ion	$\frac{d[H_3O^+]}{dt} = -\frac{J_{H_3O^+}}{V_{aq}} + r_1 + r_2$	(13)
Hydroxide ion	$\frac{d[HO^-]}{dt} = -\frac{J_{HO^-}}{V_{aq}} + r_2$	(14)
Interfacial conservation of molar flows		
Total acid conservation	$J_{AH,aq} + J_{AH,org} + J_{CPX} + J_{A^-} = 0$	(15)
Charge conservation	$J_{A^-} + J_{HO^-} - J_{H_3O^+} = 0$	(16)
Total amine conservation	$J_{R_3N} + J_{CPX} = 0$	(17)
Mass balance equation in the organic phase		
Complex	$\frac{d[CPX]}{dt} = -\frac{J_{CPX}}{V_{org}} - r_5$	(18)
Amine	$\frac{d[R_3N]}{dt} = -\frac{J_{R_3N}}{V_{org}} + r_5$	(19)
Protonated acid in the organic phase	$\frac{d[AH_{org}]}{dt} = -\frac{J_{AH,org}}{V_{org}} + r_5$	(20)

2.1.5. Definition of the parameters

2.1.5.1 Chemical equilibrium constants

Chemical equilibrium constants are known from the literature and our previous works [25,26]. At 25°C, the molarity-based dissociation constants of 3-HP and water are $K_A = 10^{-4.51}$ and $K_w = 10^{-14}$ respectively. The complexation constant at 25°C can be estimated based on the composition of the organic phase [25]:

$$\ln(K_{11}) = -6.84 + 19.7x_{ROH}^{ini} - 19.4\left(x_{ROH}^{ini}\right)^2 + 9.5\left(x_{ROH}^{ini}\right)^3 \quad (21)$$

At 20%v/v of TOA, the complexation constant can also be estimated with the working temperature (in K) [26]:

$$\ln(K_{11}) = \frac{3046}{T} - 8.091 \quad (22)$$

At 25°C and for 20%v/v of TOA, both calculations lead to K_{11} = 8.3 L.mol^{-1}.

The decanol/water partition coefficient of 3-HP (m) can be estimated with the working temperature (in K) [26]:

$$\ln(m) = -\frac{1838}{T} + 2.267 \quad (23)$$

At 25°C, this formula leads to m=0.020.

2.1.5.2. Reaction rate constants

This process is assumed to be driven by diffusion in boundary layers and especially in membrane pores. Accordingly, we assume that bulk chemical reactions are not limiting. Therefore, the backward reaction rate constants R_{-1}, R_{-2} and R_{-5} were set high enough not to influence the transfer rate. They were arbitrarily set to 10^6 L.mol^{-1}.s^{-1} in the computations.

2.1.5.3. Mass transfer coefficients

The mass transfer coefficient in the aqueous boundary layer was estimated using a relation known as Lévêque's solution correlating Sherwood number with Reynolds and Schmidt numbers [27]. The contribution of boundary layers in the global mass transfer resistance is expected to be minimal compared to the membrane pores. Accordingly, we assume correlations to be enough for this estimation. For the aqueous phase in the fibers, Lévêque relation leads to:

$$k_{X,aq} = 1.62 \times \left(\frac{v_{aq} D_{X,aq}^2}{L d_{in}}\right)^{\frac{1}{3}} \quad (24)$$

The diffusion coefficient is estimated using the Wilke-Chang correlation [28] applied to water as solvent:

$$D_{X,aq} = 7.4\ 10^{-8} \times \frac{\left(2.6 M_{H_2O}\right)^{\frac{1}{2}} T}{\mu_{aq} v_X^{0.6}} \quad (25)$$

With M_{H_2O} the molecular weight of water (g.mol^{-1}), T the temperature (K), μ_{aq} the viscosity of the aqueous phase (mPa.s) and v_X the molar volume of the considered solute (cm^3.mol^{-1}).

As mentioned above, the organic phase inside ~~in~~ the membrane pores is stagnant (no convection).

Therefore, transport phenomena are supposed to be driven by one-dimensional diffusion in pores, whose length is much higher than the average diameter (approximately 3000 times) without mass accumulation. We assume this to be the limiting step of mass transfer given the high flowrates used. In such conditions, the mass transfer coefficient should be proportional to the diffusion coefficient of the species. However, as the tortuosity and the porosity of the membrane as well as the diffusion coefficients are not precisely measured values, a preliminary extraction experiment is necessary to estimate an aggregate parameter defined as the product [mass transfer coefficient ($m.s^{-1}$) × available surface (m^2)], obtained by comparing model predictions with the results of the experiment. For the sake of clarity, the product [mass transfer coefficient × available surface, $k_i S_{org}$] is called "volumetric mass transfer coefficient" ($m^3.s^{-1}$). Actually, only the volumetric mass transfer coefficient of the complex is determined in that way, the other ones were derived from it using the following relationship based on the Wilke-Chang correlation and the assumption that the organic volumetric mass transfer coefficient is proportional to the corresponding diffusion coefficients (see calculations in appendix A):

$$k_i S_{org} = k_{CPX} S_{org} \times \left(\frac{v_{CPX}}{v_i}\right)^{0.6} \qquad (26)$$

With i being here either AH_{org} or R_3N.

In our former experiments, we could observe that the viscosity of organic phases highly concentrated in complex increased significantly. This observation corroborates Kohler et al [29] who studied the thermodynamics of the acetic acid/triethylamine mixture and found that, when adding triethylamine (0.36 mPa.s, 25°C) in acetic acid (1.1 mPa.s, 25°C), the viscosity had a bell-shape profile. It increases sharply at the beginning and reaches a maximum value 15 times higher (16.7 mPa.s, 25°C) than the original acetic acid viscosity for a specific mixture composition. Juang et Chen [21] found significant deviations between their dynamic model of membrane extraction and their experimental results for lactic acid concentrations above 4 $g.L^{-1}$ and attributed this observation to potential viscosity effects.

As the complex concentration may vary significantly with time, we decided to take this phenomenon into account. If we assume that the temperature remains constant, we can consider, for a species i, the product between μ and D as invariant based on Wilke-Chang relation (25):

$$D_{i,org}(C_{org})\mu_{org}(C_{org}) = D^0_{i,org} \times \mu^0_{org} \quad (27)$$

Where $D^0_{A,org}$ and μ^0_{org} are reference values known for a given acid concentration, for example $C_{org} = 0$.

The concentration gradient along the membrane pores induces a viscosity gradient which leads to a variation in volumetric mass transfer coefficient along the pores. However, if we assume that this coefficient is proportional to the diffusion coefficient and that the variation of the viscosity depends linearly on the acid concentration (see section 3.1.), it is possible to find a relation for an average volumetric mass transfer coefficient on the organic side (see appendix B):

$$\overline{k_{m,A}}(t)S_{org} = k^0_{m,A}S_{org} \times \frac{\mu^0_{org}}{\mu_{org,lm}(t)} \quad (28)$$

Where $\mu_{org,lm}$ is the logarithmic mean of the viscosity between the inlet and the outlet of the membrane pores:

$$\mu_{org,lm} = \frac{\mu_{bulk} - \mu_{int}}{\ln\left(\frac{\mu_{bulk}}{\mu_{int}}\right)} \quad (29)$$

The linear variation of viscosity with acid concentration will be checked in the results section.

2.1.5.4. Extraction coupled to back-extraction (pertraction)

The modeling of the pertraction system made of extraction coupled to back-extraction is similar to the extraction. The chemical reactions in the back-extraction side are the same as the extraction side but the initial acid concentration is null and sodium hydroxide (NaOH) is added. Mass balance equations in the organic phase are adapted to take into account species flows from both extraction and back-extraction contactors.

2.1.6. Initial concentration of species in each phase

Before beginning the kinetics modeling, it is necessary to determine the exact composition of each phase.

In aqueous phases, the acid is present and possibly sodium hydroxide for pH regulation and back-extraction. The determination of the equilibrium composition of a weak acid solution in combination with sodium hydroxide leads to the resolution of a cubic equation derived from the acid and water

dissociations (reactions 1 and 2), the total acid conservation and the electroneutrality principle. For example, with the dissociated acid as the unknown:

$$[A^-]^3 + \left(K_A - [Na]_0 - \left[AH_{aq}\right]_0 - \frac{K_w}{K_A}\right)[A^-]^2 + \left([Na]_0\left[AH_{aq}\right]_0 - 2K_A\left[AH_{aq}\right]_0\right)[A^-] + K_A\left(\left[AH_{aq}\right]_0\right)^2 = 0 \quad (30)$$

where $[Na]_0$ is the initial introduced concentration of sodium hydroxide. The physical solution for $[A^-]$ is the one between 0 and $[AH]_0$. All other compounds concentrations can easily be deduced from $[A^-]$. In our experiments, at the extraction side NaOH is not used and $[Na]_0 = 0$.

For the organic phase, the determination of the equilibrium composition leads to a quadratic equation derived from the equilibrium between the free and the complexed form of the acid (reaction 5) and the total acid conservation. For example, with the free form of the acid as the unknown:

$$\left[AH_{org}\right]^2 + \left(\frac{m}{K_{11}} + [R_3N]_0 - \left[AH_{org}\right]_0\right)\left[AH_{org}\right] - \frac{m\left[AH_{org}\right]_0}{K_{11}} = 0 \quad (31)$$

2.1.7. Numerical solution of model equations

Model equations were solved numerically using Matlab® software (MathWorks, Natick, MA). Since chemical reactions in the bulk phases were assumed very fast compared to mass transfer dynamics by setting reaction rate constants R_{-1}, R_{-2} and R_{-5} to very high values, the resulting system of differential equations was numerically "stiff", i.e. contained a combination of slow and fast dynamics. A stiff solver (ode15s in the Matlab ODE suite) was used for the solution of differential equations in Table 2.

2.2. Experimental strategy

First, a reactive extraction of 1 $g.L^{-1}$ 3-HP in water (500 mL) by a 20%v/v TOA in n-decanol (500 mL) was performed using a membrane contactor in a device described previously [30]. This experiment aimed to calibrate the only unknown parameter of the model, i.e. the volumetric mass transfer coefficient of the complex in the organic phase ($k_{CPX}S_{org}$). The determined value was used to simulate extraction

(and back-extraction) in different conditions and the results were compared to experimental measurements.

To get closer to fermentation conditions, 3-HP was brought into the aqueous phase at the highest rate reported in literature for 3-HP fermentation from glucose, i.e. 2.5 $g.L^{-1}.h^{-1}$ [16]. To enhance transfers, it is necessary to continuously regenerate the organic phase using a back-extraction system identical to the extraction one except that the aqueous phase is loaded with sodium hydroxide. The whole pertraction device is described in Figure 2. The experimental results were confronted to the model predictions for validation.

If 3-HP is continuously added for long enough at the specified rate, a steady state is reached in the extracted aqueous phase and in the organic phase, while 3-HP accumulates in the back-extraction phase. The model was used to predict this steady state and an experiment was performed to check the accuracy of the prediction.

2.3. Chemicals

The organic phase consisted in 20%v/v tri-*n*-octylamine (TOA) (98% purity, Sigma-Aldrich, USA) diluted in *n*-decanol (>99% purity, Sigma-Aldrich, USA) saturated with water, to minimize volume and properties variations during extractions. Before use, TOA was purified using the protocol described in [31]. The aqueous phases consisted in 3-hydroxypropionic acid (30%wt in water, TCI Europe, Belgium) and sodium hydroxide (>98% purity, Sigma-Aldrich, USA) diluted in ultrapure water.

2.4. Experimental devices and conditions

The first extraction device, a lab scale system [30], was used in the same experimental conditions as described in [30]: 25°C, aqueous and organic flowrates of 8.6 $mL.s^{-1}$ and 8.1 $mL.s^{-1}$ respectively, 0.4 bar of differential pressure between the aqueous and the organic phase, 500 mL of each phase.

The second extraction device was a fully automated pilot system built by Seprosys®, equipped with flowrate control and regulation and pH, pressure and temperature inline measurements and acquisition (0.5 Hz). Pressure was measured upstream and downstream from the modules in each phase in order to evaluate the pressure drop across the contactor. Pressure levels were then set

manually with needle valves to get a stable interface. As it can be seen in Figure 2, the set-up is similar in principle to the lab scale system described previously [30]. However, the pilot unit contains a second extraction set-up that was used as a back-extraction loop to continuously regenerate the organic phase when coupled to the extraction. All flowrates were set to 15.3 $mL.s^{-1}$. The extracted aqueous phase and organic phase volumes were set to 1 and 1.5 L respectively. The volume of the back-extraction phase was set to 650 mL, unless otherwise specified, in order to concentrate 3-HP. Depending on the experiment, the whole quantity of 3-HP was directly placed initially in the extracted aqueous vessel or gradually introduced at a specific rate of 2.5 $g.h^{-1}$ using a peristaltic pump, to mimic a microbial production. The temperature was kept constant at 25°C using jacketed vessels.

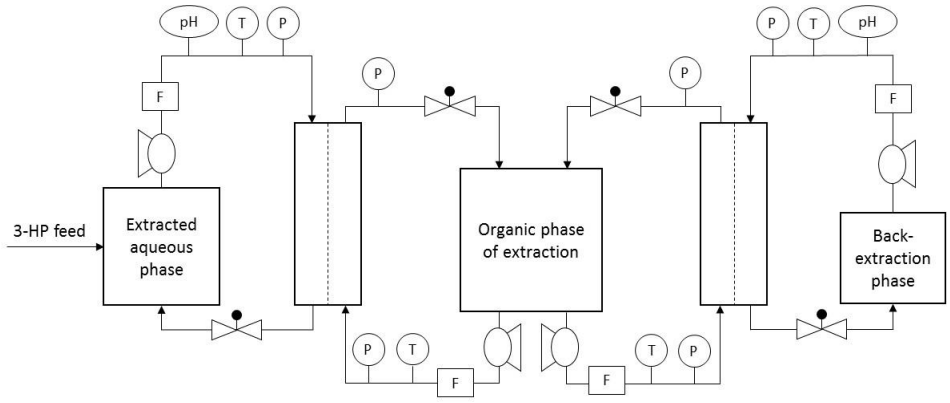


Figure 2: Process and instrumentation diagram of the plant used for extraction and back-extraction

Both the lab scale and the pilot devices were equipped each with two identical hollow-fiber membrane contactors (Liqui-Cel X50, Table 3).

Table 3: Characteristics of the Liqui-Cel commercial modules used

Module 2.5x8"		Fibers X50	
Material	Polypropylene	Material	polypropylene
Internal diameter (D)	58.4 mm	Internal diameter (d_{in})	220 µm
Internal length	20.3 mm	External diameter (d_{out})	300 µm
Number of fibers	~ 9800	Effective length (L)	146 mm
		Wall thickness	40 µm
		Porosity	~40%
		Average pore diameter	0.03 µm

2.5. Analytical methods

The viscosity of the organic phase loaded with different amounts of 3-HP was determined using a cone and plate rheometer (Rheostress 600, Thermo Scientific). A linear shear rate ramp was performed from 0 to 100 s^{-1} at 25°C. All samples displayed a Newtonian behavior, and the viscosity was determined as being the slope of the measured shear stress vs. imposed shear rate curve.

Samples were taken over time in each vessel for concentration determination using HPLC as detailed in [31]. The organic samples were first back-extracted using the same volume of a solution of sodium hydroxide in excess and the resulting aqueous phases were then analyzed.

The overall recovery yield of 3-HP in the back-extraction phase was calculated according to:

$$Y = \frac{[AH]_{BE} V_{aq}^{BE}}{[AH]_{E} V_{aq}^{E} + [AH_{org}] V_{org} + [AH]_{BE} V_{aq}^{BE}} \quad (32)$$

With *BE* meaning the back-extraction phase and *E* the extracted phase.

Experiments have been performed in duplicate unless specified otherwise and all conditions can be found in the following Table 4 with their corresponding names.

Table 4: Summary of all the experimental conditions tested with their corresponding referring name (n.a. not applicable)

	$[AH]_E^{ini}$ (g.L^{-1})	F (g.h^{-1})	$[AH]_{org}^{ini}$ (g.L^{-1})	V_{aq}^E (L)	V_{org} (L)	V_{aq}^{BE} (L)	Q_{aq}^E (mL.s^{-1})	Q_{org} (mL.s^{-1})	Q_{aq}^{BE} (mL.s^{-1})	Device
E1	1	n.a.	0	0.5	0.5	n.a.	8.6	8.1	n.a.	Lab
E2	1	n.a.	0	1	1	n.a.	15.3	15.3	n.a.	Seprosys
E3	10	n.a.	0	1	1	n.a.	15.3	15.3	n.a.	Seprosys
E4	0	2.5	0	1	1.5	0.65	15.3	15.3	15.3	Seprosys
E5	1.6	0.5	2.6	1	1.5	0.85	15.3	15.3	15.3	Seprosys

3. Results and discussion

3.1. Experimental and corresponding modeling results

3.1.1. Viscosity measurements

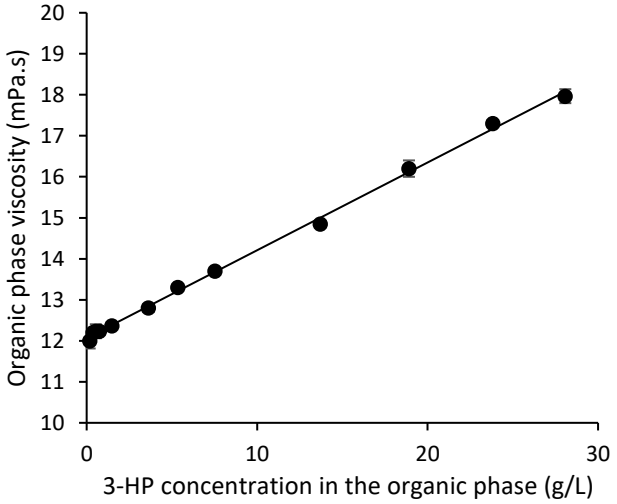


Figure 3: Organic phase viscosity as a function of 3-HP concentration (25°C)

In the range tested, a linear correlation shown in Figure 3 was found between viscosity and 3-HP concentration in the organic phase (20% TOA in *n*-decanol), validating the assumption made in section 2.1.5.3. :

$$\mu_{org} = 0.214 C_{org} + 12.1 \quad (R^2 = 0.998) \qquad (33)$$

Where μ_{org} is the viscosity in mPa.s and C_{org} the 3-HP concentration in the organic phase (AH_{org} + CPX) in $g.L^{-1}$. The viscosity increases by 50% when the acid concentration varies from 0 to $28 g.L^{-1}$. The knowledge of this correlation makes it possible to replace μ_{bulk} and μ_{int} in equation (29) to obtain volumetric mass transfer coefficients using the viscosity dependency relationship (equation (28)). The system of Table 2 can then be numerically solved for concentrations using the procedure described in section 2.1.7.

3.1.2. Model calibration and simple extractions (conditions E1, E2, E3*)*

For model calibration, an extraction experiment in membrane contactor on a lab device (E1) was first carried out and the results are shown in Figure 4.

As previously mentioned, the model needs the value of $k_{CPX}S_{org}$, the volumetric mass transfer coefficient of the complex in the organic phase. The required parameters values (porosity, tortuosity …) to estimate this coefficient with theoretical and empirical relations being very uncertain, $k_{CPX}S_{org}$ was estimated based on data from a single experiment. The corresponding experiment (E1) was performed in the lab scale extraction device with 1 $g.L^{-1}$ 3-HP initially in the aqueous phase and 500 mL of each phase. $k_{CPX}S_{org}$ was found to be around 5.4 10^{-8} $m^3.s^{-1}$.

Two other extraction experiments (E2 and E3) were performed in the Seprosys® pilot device using 1L of each phase with 1 $g.L^{-1}$ and 10 $g.L^{-1}$ 3-HP respectively in the aqueous phase initially. The results of these experiments are shown in Figure 4. The value of $k_{CPX}S_{org}$ obtained above was kept the same and model simulations are also plotted in Figure 4.

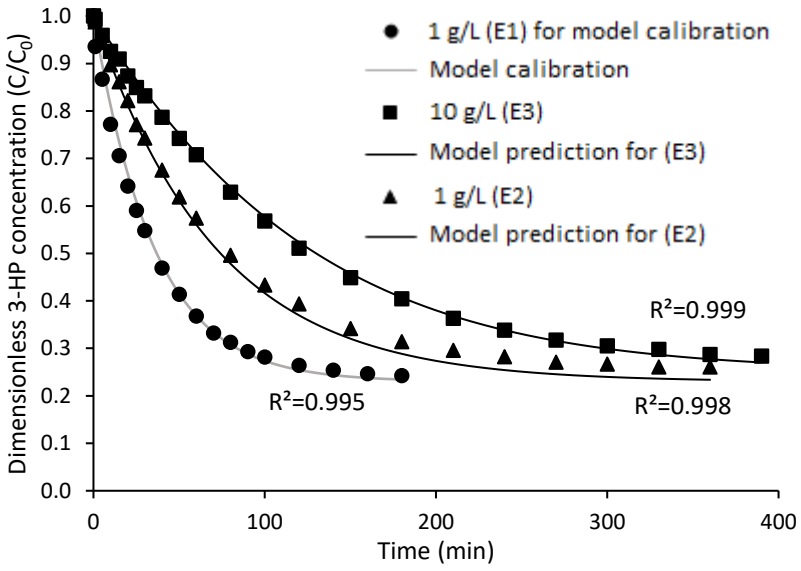


Figure 4: Experimental and model results of 3-HP extraction for different initial acid concentrations and two separate experimental devices (conditions E1, E2, E3*)*

We can see that the model-based simulations fit the experimental results very well (R^2>0.995). Comparing the extraction kinetics obtained at 1 $g.L^{-1}$ on the two separate devices, the Seprosys® device gave much slower extraction ($E2, E3$) than the lab scale device ($E1$). This is because the volume of the extracted phase was doubled while the surface area of the membrane module remained the same.

Noting that the flow rate of each phase was practically doubled compared to the calibration experiment, one can reasonably conclude that the global mass transfer is mainly governed by the diffusion in the pores of the membrane and that the contribution of phases' boundary layers is negligible.

3.1.3. Gradual addition of 3-HP (condition $E4$)

In order to simulate a production of acid through a fermentation, 3-HP was gradually fed to the extracted vessel at a rate of 2.5 $g.h^{-1}$. To limit 3-HP accumulation, the organic phase was continuously regenerated with a 20 $g.L^{-1}$ sodium hydroxide solution using a second contactor module as shown in Figure 2. The organic phase volume had to be increased in order to fill both the extraction and the back-extraction circuits. The experimental concentrations of the 3 phases and their corresponding model predictions are plotted against time in Figure 5 where 3-HP under all forms: dissociated and undissociated 3-HP in aqueous phases ($[AH_{aq}] + [A^-]$) and complexed and free 3-HP ($[CPX] + [AH_{org}]$)in the organic phase.

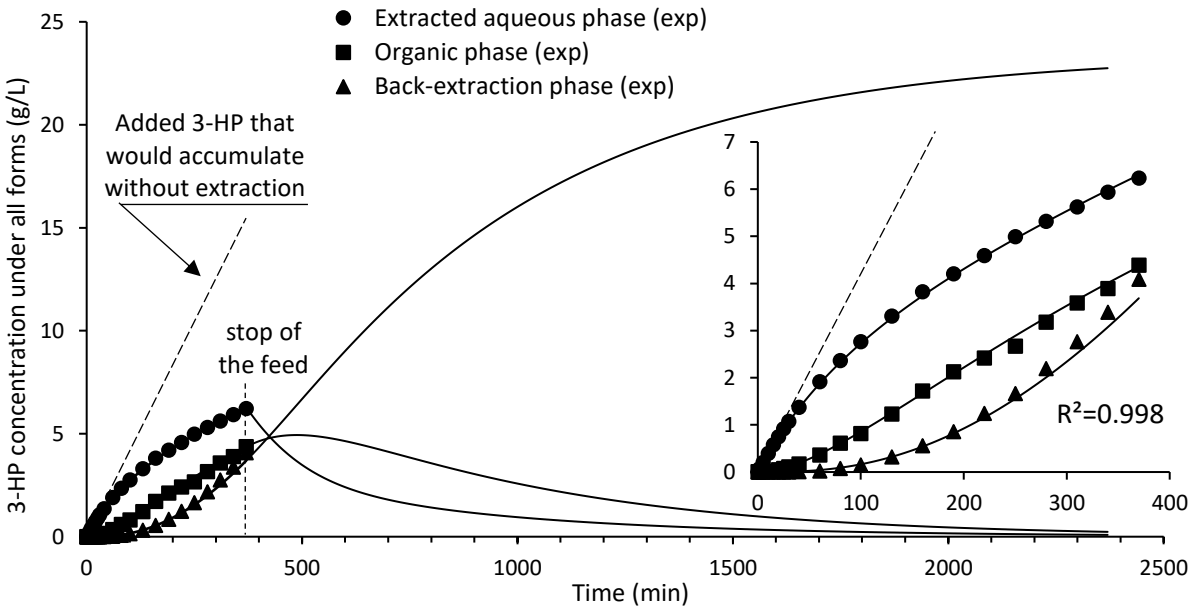


Figure 5: Experimental and simulated concentration evolution in the three phases during gradual 3-HP addition in the extracted phase (condition $\mathrm{E4}$*) ; inset: zoom on the first 370 minutes for which frequent experimental measurements were performed*

Here again, it is obvious that the model predicts correctly (R^2=0.998) the experimental evolution of 3-HP concentration in each phase during the first 370 minutes which is a good validation of the model in 3-HP feeding conditions.

However, we can see the acid accumulating over time in the 3 phases. Indeed, the extraction was not efficient enough to compensate the addition of 3-HP at a feed rate of 2.5 $g.h^{-1}$. At 370 min, 3-HP concentration in the extracted aqueous phase reached 6.2 $g.L^{-1}$, while 15.2 g of 3-HP were added to the system within the same time. This means the extraction unit was able to divide by 2.5 the concentration in the extracted phase compared to a system without extraction. The acid accumulation in a totally non-buffered medium led to an important decrease in pH which was correctly predicted by the model (see Figure 6A) using the formula:

$$pH = -\log([H_3O^+]) \quad (30)$$

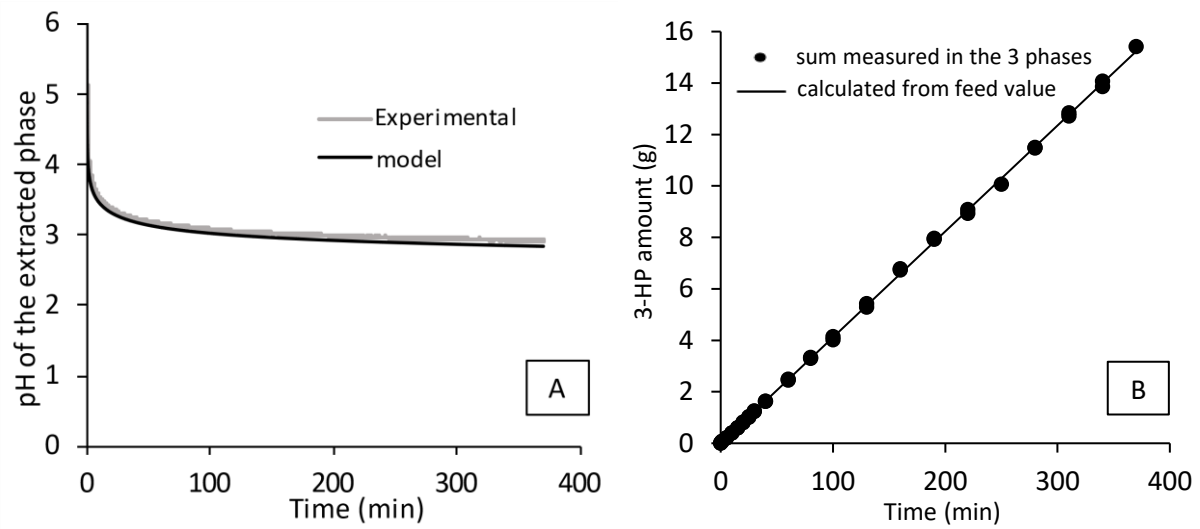


Figure 6: (A) Predicted and experimental pH evolution in the extracted phase with gradual 3-HP addition (condition E4*) . (B) Calculated and measured amount of 3-HP in the system against time (condition* E4*)*

After 370 min, the feed was stopped, and the system was allowed to reach equilibrium during 4 days just letting the streams circulate in the device with the applied flowrates.

The model predicted a total depletion of the extracted and the organic phases while the entire amount of 3-HP accumulated in the back-extraction phase. Experimentally, after the 4 days, only few of 3-HP (around 0.1 $g.L^{-1}$) could be detected in the extracted phase while the back-extraction phase reached a concentration of 23.9 $g.L^{-1}$ and no 3-HP was left in the organic phase. This concentration is 1.57 times higher than what should have been found in the extracted phase without extraction and it corresponds to a volume ratio of 1.54 between the extracted and the back-extraction phases. As the near totality of the product was recovered in the back-extraction step, the volume ratio determines the concentration factor. This is quite interesting for product concentration purposes. In the considered configuration, the concentration of the 3-HP in the back-extraction phase was mainly limited by the NaOH concentration, as the back-extraction reaction is total. The overall recovery yield of 3-HP in the back-extraction phase exceeded 99%.

Considering the experimental mass balance (Figure 6B), it appears that, on average, the total amount of 3-HP measured in the system is 100 ± 2% of the theoretical amount brought by the feed. We can consider that all the 3-HP in the system was quantified. Therefore, for the experiments presented

below, only the concentrations in the extracted and the back-extracted phases were determined and the concentrations in the organic phase were deduced from the mass balance and the applied feed.

3.1.4. Steady state experiment (condition E5)

In order to check the possibility of a steady state in the extracted vessel using our experimental system, we decided to change the initial conditions in this experiment to get a steady state directly from the beginning of the experiment. We used the predictive model in order to find such conditions. The selected conditions were the following:

- 3-HP feed rate: 0.5 $g.h^{-1}$
- initial 3-HP concentration in the extracted phase: 1.6 $g.L^{-1}$
- initial 3-HP concentration in the organic phase: 2.6 $g.L^{-1}$

The volumes were the same as for the previous experiment except for the back-extraction, and the evolution of 3-HP concentration in both aqueous phases were measured over time.

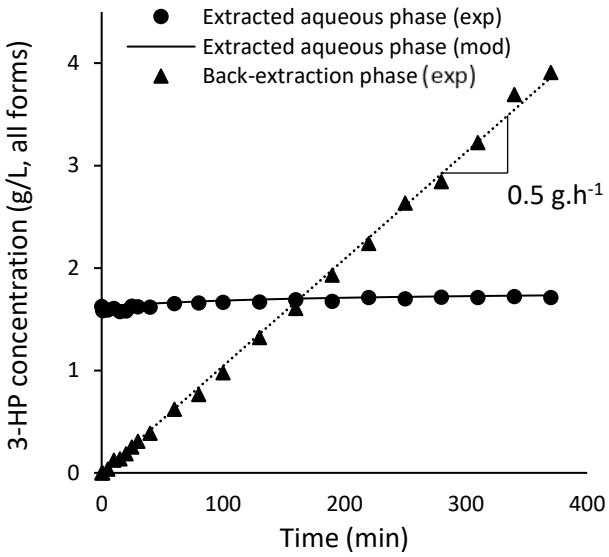


Figure 7: Concentration evolution in the extracted and the back-extraction phases in the steady-state experiment conditions (condition E5; dotted line: linear regression for slope calculation)

Figure 7 shows a very good agreement between the model prediction and the experimental data. In the extracted phase, 3-HP concentration remained constant over time. Accordingly, the concentration in the back-extraction phase increased linearly, becoming higher than the concentration in the extracted phase. The slope of the linear regression led to the 3-HP accumulation rate in the back-extraction phase of 0.5 $g.h^{-1}$. This is the same value as the feed rate indicating that all the added 3-HP accumulated in the back-extraction phase. This demonstrates the ability of the system to keep a constant concentration in the extracted aqueous phase while concentrating the product in the aqueous back-extraction phase when 3-HP is produced. In the conditions of section 3.1.3., according to our model, a steady 3-HP concentration in the extracted phase of 29 $g.L^{-1}$ would be reached if NaOH remained not limiting.

3.2. Model-based exploration of mass transfer mechanisms

3.2.1. Viscosity effects on the mass transfer coefficient of the complex

First, the viscosity effects are studied in the case of a simple extraction with a given concentration of 3-HP in the aqueous phase as in section 3.1.1. Figure 8 shows the evolution of the 3-HP dimensionless concentration along time during a simple extraction (without back-extraction) with different initial concentrations in order to evaluate the 3-HP concentration effect on the extraction kinetics and to assess the accuracy of the model concerning the influence of the viscosity.

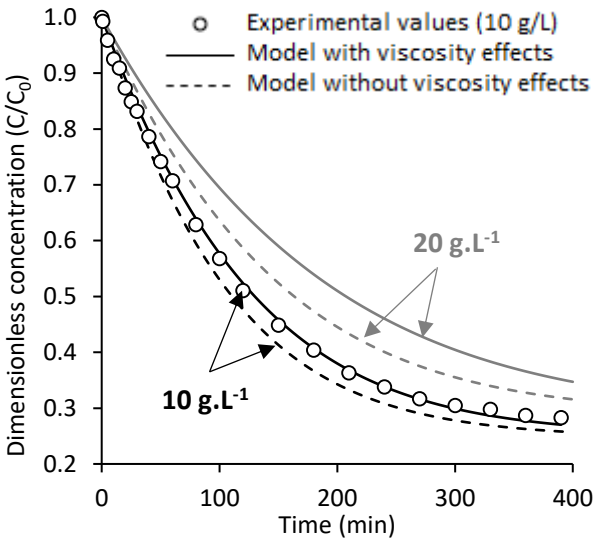


Figure 8: Evolution of 3-HP concentration in the extracted aqueous phase for different initial concentrations in a simple extraction mode without back-extraction (symbols: experimental points only for 10 g/L 3-HP in condition E3, lines: model predictions)

At weak initial concentrations, viscosity effects are negligible but, at 10 $g.L^{-1}$ 3-HP initially, differences in predictions between models are already significant with the viscosity effects slowing down the extraction compared to a model where the viscosity is kept constant at the initial value. At 1$g.L^{-1}$, the 2 models provide the same results. Indeed, at this low level, acid concentration in the organic phase is low and the viscosity and the mass transfer coefficient are not impacted significantly. However, at 10 $g.L^{-1}$, the model including viscosity effects gets closer to experimental results. Including the viscosity effects, the modeled characteristic time of extraction increases by 17% from 95 (without viscosity effects) to 111 min (with viscosity effects) and fits better the experimental results. Increasing more the initial concentration, e.g. at 20 $g.L^{-1}$, increases the difference in predictions between these models, with a difference in characteristic times of 27% from 135 (without viscosity effects) to 171 min (with viscosity effects). This demonstrates the necessity to consider viscosity effects at high 3-HP concentration.

Using the model, it is possible to estimate the interfacial concentrations for all the species and specifically of acid in the aqueous phase, TOA and complex in the organic phase, as shown on Figure 9. These concentrations cannot be measured directly in the considered membrane contactor.

Immediately after starting the extraction, 3-HP and TOA bulk concentrations are set by initial conditions and the one of the complex is null. However, close to the interface, TOA and 3-HP are consumed so that their concentrations are lower than in the bulk. This clearly appears in Figure 9 for TOA but for 3-HP in aqueous phase the mass transfer resistance is negligible and the interfacial and bulk concentrations are very close. The complex concentration is higher at the interface than in the bulk as it is formed at the interface. As time passes, interfacial and bulk concentrations get closer and become equal when the equilibrium is reached, because mass transfer fluxes across the boundary layers become zero.

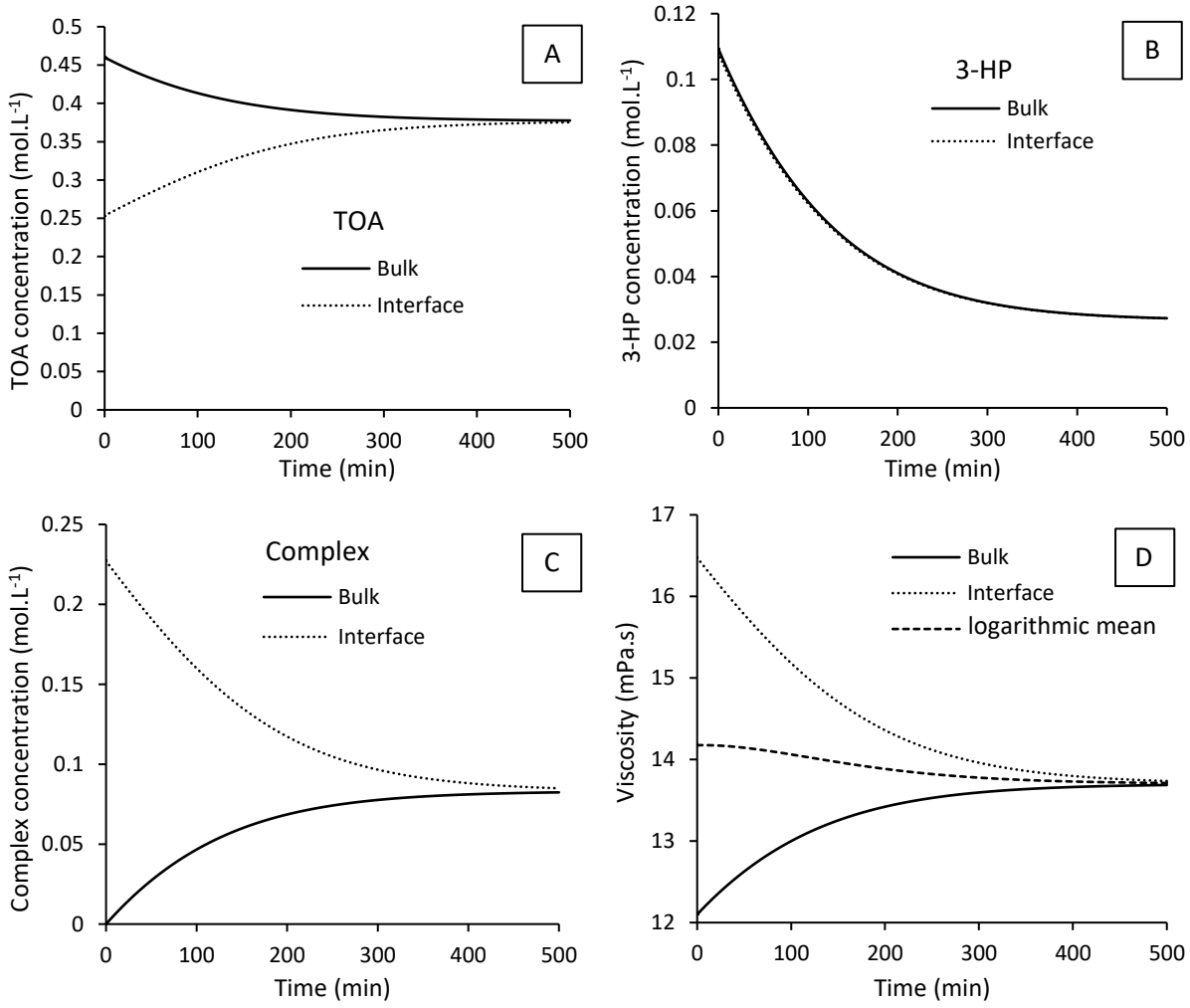


Figure 9: Computed variation of TOA (A) and Complex (C) concentrations in the organic phase and of non-dissociated 3-HP concentration (B) in the aqueous phase close to the liquid-liquid interface and in the corresponding bulk along time ; organic phase viscosity variation (D) near the interface and in the bulk along time according to the model (condition E3)

The higher complex concentration at the interface generates a higher viscosity compared to the bulk. However, as the interfacial viscosity decreases while the one of the bulk increases over time, their logarithmic mean stays almost constant and the mass transfer coefficient in the membrane should essentially be constant over time (Figure 14D). Even if the viscosity is rather constant, its value is still 15% higher than with very dilute 3-HP. Figure 10 provides the evolution of the membrane mass transfer coefficient for different inital 3-HP concentrations (k), relative to the case of very dilute 3-HP (k_0). As expected, an increase in the initial concentration leads to a decrease of the mass transfer coefficient. As already explained, the coefficient does not vary greatly over time. For all the cases plotted (without back extraction and with similar extracted and organic phase volumes), the approximation of a constant mass transfer coefficient can be sufficient.

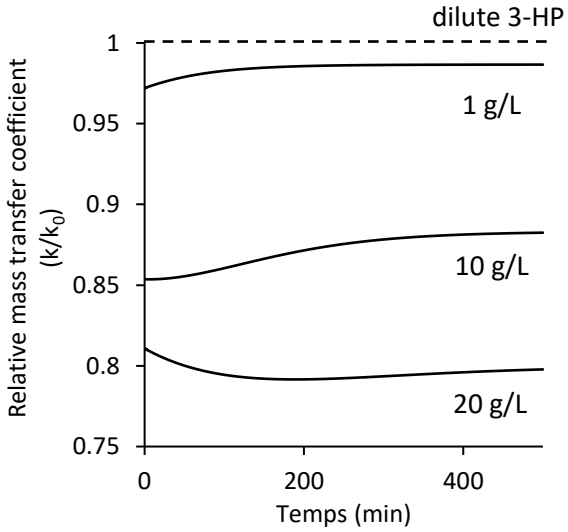


Figure 10: relative mass transfer coefficient variation along time for a simple extraction without back-extraction using different initial 3-HP concentrations in the aqueous phase according to the model (k_0 mass transfer coefficient for very dilute 3-HP)

Another example demonstrates the necessity to consider the viscosity effects. Experimental and model results in the conditions of section 3.1.3. (gradual addition of 3-HP at 2.5$g.L^{-1}.h^{-1}$) are provided in Figure 11. Once again, it is obvisous that viscosity effects impact the transfer and considering them is necessary to get better predictions of concentrations variations. Due do the progressive addition of 3-HP, the mass transfer coefficient decreases along time and at 8h of experiment a decrease of 17% is

predicted and confirmed by the results. In this case, the assumption of a constant mass transfer coefficient is not appropriate.

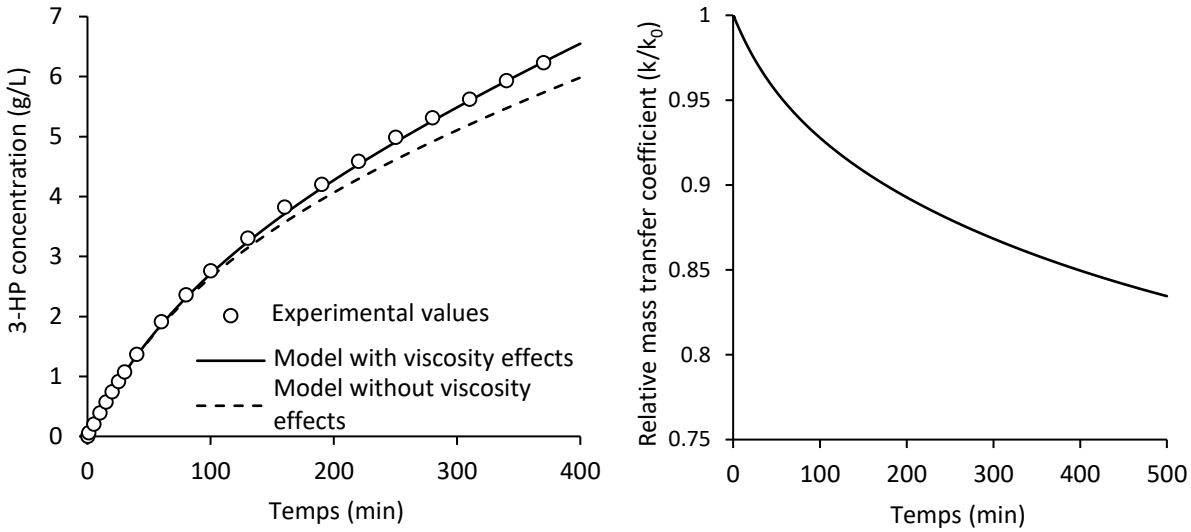


Figure 11: (A) Evolution of the 3-HP concentration in the aqueous phase along time with a gradual feed when extraction and back-extraction are coupled as in condition E4 (symbols: experimental values, lines: models). (B) Evolution of the mass transfer coefficient in the same experiment according to the model

3.2.2. Model-based guidelines for the selection of the extracting phase

The model presented here relies on only 2 main experimentally determined parameters: the complexation equilibrium constant (K_{11}) and the organic phase viscosity (μ). It is then possible to extrapolate the results of the model to address other couples (K_{11} ; μ) and use it as a tool to select a viable system of extraction considering a design requirement. For example, the highest 3-HP concentration reached at steady-state conditions in the bioreactor can be a meaningful requirement for the set-up of an *in-situ* product recovery as the concentration of 3-HP sets the level of inhibition on the producing microorganism.

In the following calculations (Figure 12), physical partitioning of the acid was neglected compared to reactive extraction.

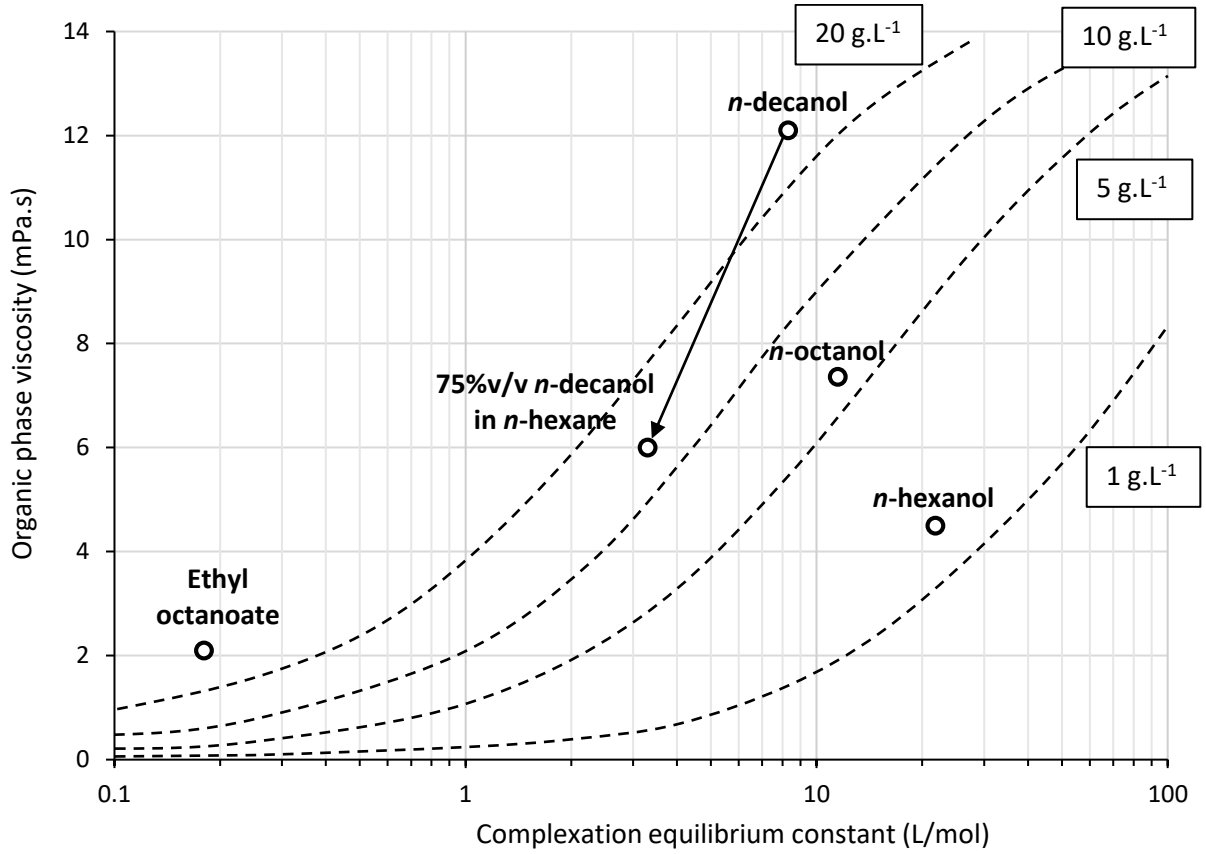


Figure 12: Nomogram based on the model allowing the estimation of the steady-state 3-HP concentration in the extracted aqueous phase in condition E4 as a function of the complexation equilibrium constant and the organic phase viscosity. Organic phases contained 20% TOA in different solvents. Symbols : solvents positions in this space)

Figure 12 shows steady-state iso-concentration curves: one curve is the set of (K_{11} ; μ) values leading to the same 3-HP concentration in the bioreactor at steady-state in the conditions of section 3.1.3 (E4). This concentration is specified along the corresponding curve. The symbols indicate the position of various solvents in the (K_{11} ; μ) space based on data from [31] and new similar measurements. Being above an iso-concentration curve means that the predicted steady-state concentration will be higher than the corresponding value. Being below means that it will be lower.

This kind of graph is useful for the formulation of an extracting system when process settings (membranes surface, phases volumes etc.) are known. In most of the studies, the main parameter considered when selecting the solvent was the extraction yield (corresponding to an equilibrium

constant), the highest yield being preferred. Our results (Figure 12) demonstrate that, for the same steady-state concentration target, a lower equilibrium constant can be compensated by a lower viscosity of the organic phase. For example, addition of hexane to decanol (arrow on Fig 12) decreases the viscosity more than the equilibrium constant relative to the steady-state iso-concentration curves. This means that adding hexane to decanol will decrease the final accumulation of 3-HP in the bioreactor despite the decrease of the distribution equilibrium of 3-HP between the aqueous and the organic phases.

4. Conclusion

In this work, we developed a dynamic model to simulate 3-hydroxypropionic acid reactive extraction using tri-*n*-octylamine in decanol in membrane contactors. This model mainly relies on instantaneous species complexation at the aqueous-organic phases interface and diffusion in the membrane pores filled with the organic phase. For the sake of modeling accuracy, the increase in viscosity as a function of the acid concentration in the organic phase (up to 50% at 28 g/L of 3-HP) has been considered for the first time. Hence, the model includes an organic mass transfer coefficient taking into account acid concentration variation with time and along the membrane pore. The model was proved to be predictive and accurate (R^2>0.99) in the case of forward reactive extraction and was extended to include simultaneous extraction and back-extraction using sodium hydroxide with an additional membrane contactor to regenerate the organic phase, allowing to represent the whole pertraction process. The model accurately predicted the coupling of extraction and back-extraction systems in transient and steady state regimes (R^2>0.99 for all the experiments). No need was found to take specific chemical kinetics and interfacial resistance into account.

The model will be very useful to formulate new extraction systems for example to further enhance the selectivity or reduce toxicity while maintaining good extraction performances for given process settings. Moreover, for a given formulation of the extraction system, this model would be very helpful in sizing process settings like the membranes surface area. However, in order to really consider an implementation as an *in stream* product recovery, further interactions between real bioconversion

media and the extraction system need to be better understood. This subject is at the heart of the current concerns of our research team.

Appendix A: Determination of mass transfer coefficients of other solutes based on the mass transfer coefficient of the acid-amine complex in the membrane

If we assume that, everything else being equal, the mass transfer coefficient of a solute is proportional to its diffusion coefficient, then:

$$\frac{k_i}{D_i} = \frac{k_{CPX}}{D_{CPX}} \quad or \quad k_i = \frac{D_i}{D_{CPX}} k_{CPX}$$

The Wilke-Chang correlation states that the diffusion coefficient is inversely proportional to the molar volume of the solute at the power 0.6 (equation 25). Considering the ratio of diffusion coefficients, the coefficient of proportionality cancels out and the mass transfer coefficient of a species i can be expressed as:

$$k_i = \left(\frac{v_{CPX}}{v_i}\right)^{0.6} k_{CPX}$$

Appendix B: Average mass transfer coefficient in the membrane pores

The variation of viscosity and of the diffusion coefficient of a species i are inversely proportional (equation 25), which leads to:

$$D_{i,org}(C_{org}) = D^0_{i,org} \times \frac{\mu^0_{org}}{\mu_{org}(C_{org})}$$

where $D^0_{i,org}$ and μ^0_{org} are reference values known for a given acid concentration, for example $C_{org} = 0$.

The variation of the membrane mass transfer coefficient with concentration is then similarly given by:

$$k_{i,m}(C_{org}) = k^0_{i,m} \times \frac{\mu^0_{org}}{\mu_{org}(C_{org})}$$

The concentration gradient along the membrane pores induces a diffusion coefficient variation which leads to a variation of mass transfer coefficient along the pores. It is thus possible to find a relation for an average mass transfer coefficient along the pores:

$$\overline{k_{i,m}} = \frac{1}{C_{bulk} - C_{int}} \int_{C_{int}}^{C_{bulk}} k_{i,m}(C)dC = \frac{k^0_{i,m}\mu^0_{org}}{C_{bulk} - C_{int}} \int_{C_{int}}^{C_{bulk}} \frac{dC}{\mu_{org}(C)}$$

As the viscosity is an affine function of the concentration (equation 33), this leads to:

$$\overline{k_{i,m}}(t) = k_{i,m}^{0} \times \frac{\mu_{org}^{0}}{\mu_{org,lm}(t)}$$

where $\mu_{org,lm}$ is the logarithmic mean of the viscosity between the inlet and the outlet of the pores

Funding:

This work was supported by the Institut National de Recherche pour l'Agriculture, l'Alimentation et l'Environnement (INRAE), Région Grand-Est, Conseil départemental de la Marne and Reims Métropole.

References

[1] A.S. Kertes, C.J. King, Extraction Chemistry of Fermentation Product Carboxylic Acids, Biotechnology and Bioengineering. 28 (1986) 269–282.

[2] National Research Council, Separation and Purification: Critical Needs and Opportunities, The National Academies Press, Washington, DC, 1987.

[3] A.M. Baniel, A.M. Eyal, J. Mizrahi, B. Hazan, R.R. Fisher, J.J. Kolstad, B.F. Stewart, Lactic acid production, separation and/or recovery process, US 5,510,526, 1996.

[4] B.I. Veldhuis-Stribos, J. Van Breugel, W.J. Groot, B.M. Dierdorp, Continuous process for preparing lactic acid, WO 01/27064 A1, 2001.

[5] K. Ye, S. Jin, K. Shimizu, Performance improvement of lactic acid fermentation by multistage extractive fermentation, Journal of Fermentation and Bioengineering. 81 (1996) 240–246.

[6] V.M. Yabannavar, D.I.C. Wang, Extractive fermentation for lactic acid production, Biotechnology and Bioengineering. 37 (1991) 1095–1100.

[7] M.-T. Gao, T. Shimamura, N. Ishida, E. Nagamori, H. Takahashi, S. Umemoto, T. Omasa, H. Ohtake, Extractive lactic acid fermentation with tri-n-decylamine as the extractant, Enzyme and Microbial Technology. 44 (2009) 350–354.

[8] M. Matsumoto, M. Nishimura, Extractive Fermentation of Lactic Acid with Hiochi Bacteria in a Two-Liquid Phase System, Fermentation Technology. 5 (2016).

[9] V.P. Lewis, S.T. Yang, A novel extractive fermentation process for propionic acid production from whey lactose, Biotechnology Progress. 8 (1992) 104–110.

[10] Z. Wu, S.-T. Yang, Extractive fermentation for butyric acid production from glucose byClostridium tyrobutyricum, Biotechnology and Bioengineering. 82 (2003) 93–102.

[11] Z. Gu, D.A. Rickert, B.A. Glatz, C.E. Glatz, Feasibility of propionic acid production by extractive fermentation, Le Lait. 79 (1999) 137–148.

[12] M.S. Solichien, D. O'Brien, E.G. Hammonf, C.E. Glatz, Membrane-based extractive fermentation to

produce propionic and acetic acids: Toxicity and mass transfer considerations, Enzyme and Microbial Technology. 17 (1995) 23–31.

[13] Z. Jin, S.-T. Yang, Extractive fermentation for enhanced propionic acid production from lactose by Propionibacterium acidipropionici, Biotechnology Progress. 14 (1998) 457–465.

[14] R. Nelson, D. Peterson, E. Karp, G. Beckham, D. Salvachúa, Mixed Carboxylic Acid Production by Megasphaera elsdenii from Glucose and Lignocellulosic Hydrolysate, Fermentation. 3 (2017) 10.

[15] C. Miller, A. Fosmer, B. Rush, T. McMullin, D. Beacom, P. Suominen, Industrial Production of lactic acid, in: Comprehensive Biotechnology, 2nd ed., Elsevier, 2011: pp. 179–188.

[16] T.W. Abraham, E. Allen, J.J. Hahn, P. Tsobanakis, E.C. Bohnert, C.L. Frank, Recovery of 3-hydroxypropionic acid, US 2016/0060204 A1, 2016.

[17] H.J. Jessen, B. Rush, J. Huryta, B. Mastel, A. Berry, D. Yaver, M. Catlett, M. Barnhart, Composition and methods for 3-hydroxypropionic acid production, US 2012/0135481 A1, 2012.

[18] J.G. Crespo, I.M. Coelhoso, R.M.C. Viegas, Membrane contactors: Membrane separations, in: Encyclopedia of Seperation Science, 2000: pp. 3303–3311.

[19] R. Basu, K.K. Sirkar, CITRIC ACID EXTRACTION WITH MICROPOROUS HOLLOW FIBERS, Solvent Extraction and Ion Exchange. 10 (1992) 119–143.

[20] R. Basu, K.K. Sirkar, Hollow fiber contained liquid membrane separation of citric acid, AIChE Journal. 37 (1991) 383–393.

[21] R.-S. Juang, J.-D. Chen, Mass transfer modeling of citric and lactic acids in a microporous membrane extractor, Journal of Membrane Science. 164 (2000) 67–77.

[22] H. Huang, S.-T. Yang, D.E. Ramey, A hollow-fiber membrane extraction process for recovery and separation of lactic acid from aqueous solution, in: Proceedings of the Twenty-Fifth Symposium on Biotechnology for Fuels and Chemicals Held May 4–7, 2003, in Breckenridge, CO, Springer, 2004: pp. 671–688.

[23] K.L. Wasewar, A.B.M. Heesink, G.F. Versteeg, V.G. Pangarkar, Equilibria and kinetics for reactive extraction of lactic acid using Alamine 336 in decanol, Journal of Chemical Technology &

Biotechnology. 77 (2002) 1068–1075.

[24] M.E. Marti, T. Gurkan, L.K. Doraiswamy, Equilibrium and Kinetic Studies on Reactive Extraction of Pyruvic Acid with Trioctylamine in 1-Octanol, Industrial & Engineering Chemistry Research. 50 (2011) 13518–13525.

[25] F. Chemarin, M. Moussa, F. Allais, V. Athès, I.C. Trelea, Mechanistic modelling and equilibrium prediction of organic acids reactive extraction with amines: comparative study of 2 complexation-solvation models in the case of 3-hydroxypropionic acid, Separation and Purification Technology. (2017) 475–487.

[26] F. Chemarin, M. Moussa, F. Allais, I.C. Trelea, V. Athès, Recovery of 3-hydroxypropionic acid from organic phases after reactive extraction with amines in an alcohol-type solvent, Separation and Purification Technology. 219 (2019) 260–267.

[27] A. Gabelman, S.-T. Hwang, Hollow fiber membrane contactors, Journal of Membrane Science. 159 (1999) 61–106.

[28] C.R. Wilke, P. Chang, Correlation of diffusion coefficients in dilute solutions, AIChE Journal. 1 (1955) 264–270.

[29] F. Kohler, E. Liebermann, G. Miksch, C. Kainz, Thermodynamics of the acetic acid-triethylamine system, The Journal of Physical Chemistry. 76 (1972) 2764–2768.

[30] F. Chemarin, V. Athès, M. Bedu, T. Loty, F. Allais, I.C. Trelea, M. Moussa, Towards an in situ product recovery of bio-based 3-hydroxypropionic acid: influence of bioconversion broth components on membrane-assisted reactive extraction, Journal of Chemical Technology & Biotechnology. 94 (2018) 964–972.

[31] F. Chemarin, M. Moussa, M. Chadni, B. Pollet, P. Lieben, F. Allais, I.C. Trelea, V. Athès, New insights in reactive extraction mechanisms of organic acids: An experimental approach for 3-hydroxypropionic acid extraction with tri-n-octylamine, Separation and Purification Technology. 179 (2017) 523–532.